

doi: 10.15407/ujpe60.07.0634

YU.V. KRYUCHENKO, D.V. KORBUTYAK

V.E. Lashkaryov Institute of Semiconductor Physics, Nat. Acad. of Sci. of Ukraine
(41, Prosp. Nauky, Kyiv 03028, Ukraine; e-mail: kryuchenko@isp.kiev.ua)**EXCITONIC EMISSION OF HYBRID
NANOSYSTEM “SPHERICAL SEMICONDUCTOR
QUANTUM DOT + SPHERICAL
METAL NANOPARTICLE”**PACS 73.20.Mf, 73.22.Lp,
78.20.Bh, 78.67.Bf

The hybrid nanosystem composed of a spherical metal nanoparticle (NP) and a spherical semiconductor quantum dot (QD) of a direct-band semiconductor with a cubic lattice structure and a fourfold degenerate valence band Γ_8 has been studied. The excitonic emission of the system is considered as a sum of contributions from point dipoles located at the QD lattice sites. The description of the QD + NP nanosystem, nonspherical as a whole, is based on using three spherical coordinate systems and finding the relations between the coefficients of multipole expansions of electromagnetic (EM) fields in those systems. The origins of two of them are fixed at the centers of NP and QD, and their polar axes are directed along the line connecting the centers. The orientation of the third coordinate system with the origin in the QD is determined by the orientation of the QD crystal lattice. It is shown that, unlike the electric scalar potential, which is induced by the exciton state in the QD and looks like a point-dipole potential, the EM field of the QD excitonic emission cannot be represented as that of a point dipole emission, because it contains only dipole, quadrupole, and octupole components. The multiple scattering, between the NP and the QD, of the EM field emitted by the QD is taken into account. The dependences of the excitonic emission efficiency on the separation distance between the QD and the NP surfaces are calculated in a particular case of the CdTe QD and a silver or gold NP for various QD and NP sizes and temperatures.

Keywords: quantum dot, metal nanoparticle, hybrid nanosystem, electromagnetic field, emission quantum yield.

1. Introduction

In the last years, the hybrid metal-semiconductor nanostructures (see, e.g., reviews [1,2]), in which the exciton-plasmon interaction plays a substantial role, have attracted the increasing interest owing to their unique properties and a considerable progress in the technologies of their manufacture. However, in many cases, the theoretical models used for the description of those structures are imperfect. This concerns even such simple, at first sight, case as a semiconductor quantum dot (QD) in a vicinity of a metal nanopar-

ticle (NP). In this case, the QD, by analogy with fluorescent molecules, is considered to be a point-like dipole (in such an approach, the nonspherical nanosystem transforms into the spherically symmetric one), and all well-known results obtained for the case of point dipole are automatically duplicated for the case with the QD.

In this work, which is a continuation of our previous work [3], a more rigorous approach is developed. In its framework, the whole QD is not considered as a point dipole; instead, this role is played by every elementary cell in the QD crystal. This approach makes it possible to account for the valence band structure

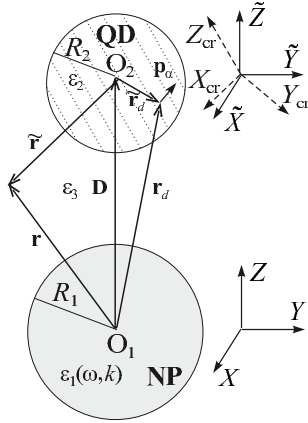


Fig. 1. Schematic diagram of the nanosystem QD + NP

in the crystal and calculate all electromagnetic (EM) fields and the emission quantum yield in the hybrid nanosystem QD + NP in the case of nonresonance excitation, when only the QD is excited directly (in the case of resonance excitation, the NP is excited directly as well). In work [3], the expressions for all EM fields in the system “emitting point dipole in a semiconductor QD + metal NP” were obtained. It was shown that, in order to calculate the EM fields in the case of QD excitonic emission in general, it is necessary to integrate the contributions made by all point dipoles in the QD to the EM fields (i.e. the contributions of all elementary cells that compose the QD crystal). It was also shown that the corresponding contributions are determined by the envelope exciton wave function in the QD.

Hence, for the further consideration, we must specify a QD model and write down the envelope exciton size-quantized wave functions. Such specification demands that, in addition to two spherical coordinate systems shifted with respect to each other by a distance D between the QD and NP centers (at the previous stage, the relations between multipole components of the EM fields expressed in those two coordinate systems were established, which enabled the spherical symmetry of QD and NP to be used separately, despite that the whole system QD + NP is not spherical), a third coordinate system $\{X_{cr}, Y_{cr}, Z_{cr}\}$ should be introduced, whose axes are defined by the orientation of the crystal lattice in the QD (see Fig. 1). The initial exciton size-quantized wave functions in the QD have a standard form just in this crystal coordinate system. However, the final exciton

wave functions, which are required for the calculation of the contribution made by the whole QD volume to EM fields, should be expressed in the coordinate system $\{\tilde{X}, \tilde{Y}, \tilde{Z}\}$ with the axis \tilde{Z} directed along the line connecting the NP and QD centers rather than the own (crystal) coordinate system with the axes $\{X_{cr}, Y_{cr}, Z_{cr}\}$. The next sections contain a description of all required transformations making it possible to calculate the powers of the EM radiation emission and absorption, as well as the emission quantum yield of the hybrid nanosystem QD + NP.

2. Size-Quantized Exciton States and Exciton Wave Functions in QD

As a material of the QD, a semiconductor with the cubic lattice structure and the fourfold degenerate valence band Γ_8 is considered; in particular, it can be CdTe. In the QD made up of such semiconductor, the ground exciton size-quantized state (the state of the so-called dark excitons, which is split off by the spin-spin electron-hole exchange interaction to the interval of lower energies) is characterized by the quantum number $F = 2$ of the total exciton angular momentum. This state is fivefold degenerate with respect to the quantum numbers $F_z = \pm 2, \pm 1, 0$ of the total momentum projections on the axis Z_{cr} . The higher-energy triple degenerate state of bright excitons is characterized by the quantum number $F = 1$ of the total exciton angular momentum and the quantum numbers $F_z = \pm 1, 0$ of its projections on the axis Z_{cr} [4].

In the electron-hole representation, according to the standard momentum sum rule (see, e.g., work [5]), the wave functions of exciton size-quantized states $\Psi_{ex}^{el-h}(F, F_z; \mathbf{r}_e^cr, \mathbf{r}_h^cr)$ look like

$$\Psi_{ex}^{el-h}(2, 2; \mathbf{r}_e^cr, \mathbf{r}_h^cr) = \Psi_e^0(\mathbf{r}_e^cr) \uparrow \Psi_h^{\frac{3}{2}, \frac{3}{2}}(\mathbf{r}_h^cr), \quad (1)$$

$$\Psi_{ex}^{el-h}(2, -2; \mathbf{r}_e^cr, \mathbf{r}_h^cr) = \Psi_e^0(\mathbf{r}_e^cr) i \downarrow \Psi_h^{\frac{3}{2}, -\frac{3}{2}}(\mathbf{r}_h^cr), \quad (2)$$

$$\Psi_{ex}^{el-h}(2, 1; \mathbf{r}_e^cr, \mathbf{r}_h^cr) = \Psi_e^0(\mathbf{r}_e^cr) \times \left[\frac{\sqrt{3}}{2} \uparrow \Psi_h^{\frac{3}{2}, \frac{1}{2}}(\mathbf{r}_h^cr) + \frac{1}{2} i \downarrow \Psi_h^{\frac{3}{2}, \frac{3}{2}}(\mathbf{r}_h^cr) \right], \quad (3)$$

$$\Psi_{ex}^{el-h}(2, -1; \mathbf{r}_e^cr, \mathbf{r}_h^cr) = -\Psi_e^0(\mathbf{r}_e^cr) \times \left[\frac{\sqrt{3}}{2} i \downarrow \Psi_h^{\frac{3}{2}, -\frac{1}{2}}(\mathbf{r}_h^cr) + \frac{1}{2} \uparrow \Psi_h^{\frac{3}{2}, -\frac{3}{2}}(\mathbf{r}_h^cr) \right], \quad (4)$$

$$\Psi_{ex}^{el-h}(2, 0; \mathbf{r}_e^cr, \mathbf{r}_h^cr) = \frac{\Psi_e^0(\mathbf{r}_e^cr)}{\sqrt{2}} \times \left[\uparrow \Psi_h^{\frac{3}{2}, -\frac{1}{2}}(\mathbf{r}_h^cr) + i \downarrow \Psi_h^{\frac{3}{2}, \frac{1}{2}}(\mathbf{r}_h^cr) \right], \quad (5)$$

where

$$\uparrow = \begin{pmatrix} 1 \\ 0 \end{pmatrix} \quad \text{and} \quad \downarrow = \begin{pmatrix} 0 \\ 1 \end{pmatrix} \quad (6)$$

are the electron spin functions (spinors) corresponding to the electron spin projections $+1/2$ and $-1/2$ on the Z_{cr} -axis, $\Psi_e^0(\mathbf{r}_e^{\text{cr}}) = \rho_0^e(\tilde{r}_e)Y_{0,0}(\Omega_e^{\text{cr}})S$ is the full spatial wave function of an electron in the size-quantized ground state, $\rho_0^e(\tilde{r}_e)$ the radial part of the electron envelope wave function, S the on-site electron wave function (the localized Wannier function [6]) of the spherically symmetric s -type, \mathbf{r}_e^{cr} the spatial electron variable in the intrinsic crystal coordinate system, the electron coordinates in the coordinate system $\{\tilde{X}, \tilde{Y}, \tilde{Z}\}$ with the origin at the point O_2 are expressed by the radius vector $\tilde{\mathbf{r}}_e$ ($r_e^{\text{cr}} \equiv \tilde{r}_e$), Ω_e^{cr} are the angular variables of the electron, $\Psi_h^{M, M_z}(\mathbf{r}_h^{\text{cr}})$ is the wave function of the hole with the quantum number M of the total angular momentum and the quantum number M_z of the momentum projection on the axis Z_{cr} , \mathbf{r}_h^{cr} the spatial variable of the hole, $Y_{l,m}(\Omega)$ the normalized scalar spherical harmonics describing the angular part of the corresponding hole envelope size-quantized wave function, l the quantum number characterizing the hole orbital momentum, and m the quantum number for its projection on the corresponding axis (this is Z_{cr} in the crystal coordinate system or \tilde{Z} in the $\{\tilde{X}, \tilde{Y}, \tilde{Z}\}$ one).

Analogously, according to the same standard sum rule for momenta, the hole size-quantized wave functions $\Psi_h^{M, M_z}(\mathbf{r}_h^{\text{cr}})$ are as follows:

$$\begin{aligned} \Psi_h^{\frac{3}{2}, \frac{3}{2}}(\mathbf{r}_h^{\text{cr}}) &= \rho_0^h(\tilde{r}_h)Y_{0,0}(\Omega_h^{\text{cr}})\left|\frac{3}{2}, \frac{3}{2}\right\rangle + \\ &+ \sqrt{\frac{2}{5}}\rho_2^h(\tilde{r}_h)\left[Y_{2,2}(\Omega_h^{\text{cr}})\left|\frac{3}{2}, -\frac{1}{2}\right\rangle + \right. \\ &\left. + Y_{2,1}(\Omega_h^{\text{cr}})\left|\frac{3}{2}, \frac{1}{2}\right\rangle + \frac{1}{\sqrt{2}}Y_{2,0}(\Omega_h^{\text{cr}})\left|\frac{3}{2}, \frac{3}{2}\right\rangle\right], \quad (7) \end{aligned}$$

$$\begin{aligned} \Psi_h^{\frac{3}{2}, -\frac{3}{2}}(\mathbf{r}_h^{\text{cr}}) &= \rho_0^h(\tilde{r}_h)Y_{0,0}(\Omega_h^{\text{cr}})\left|\frac{3}{2}, -\frac{3}{2}\right\rangle + \\ &+ \sqrt{\frac{2}{5}}\rho_2^h(\tilde{r}_h)\left[Y_{2,-2}(\Omega_h^{\text{cr}})\left|\frac{3}{2}, \frac{1}{2}\right\rangle - \right. \\ &\left. - Y_{2,-1}(\Omega_h^{\text{cr}})\left|\frac{3}{2}, -\frac{1}{2}\right\rangle + \frac{1}{\sqrt{2}}Y_{2,0}(\Omega_h^{\text{cr}})\left|\frac{3}{2}, -\frac{3}{2}\right\rangle\right], \quad (8) \end{aligned}$$

$$\begin{aligned} \Psi_h^{\frac{3}{2}, \frac{1}{2}}(\mathbf{r}_h^{\text{cr}}) &= \rho_0^h(\tilde{r}_h)Y_{0,0}(\Omega_h^{\text{cr}})\left|\frac{3}{2}, \frac{1}{2}\right\rangle + \\ &+ \sqrt{\frac{2}{5}}\rho_2^h(\tilde{r}_h)\left[Y_{2,2}(\Omega_h^{\text{cr}})\left|\frac{3}{2}, -\frac{3}{2}\right\rangle + \right. \\ &\left. + Y_{2,-1}(\Omega_h^{\text{cr}})\left|\frac{3}{2}, \frac{3}{2}\right\rangle - \frac{1}{\sqrt{2}}Y_{2,0}(\Omega_h^{\text{cr}})\left|\frac{3}{2}, \frac{1}{2}\right\rangle\right], \quad (9) \end{aligned}$$

$$\begin{aligned} \Psi_h^{\frac{3}{2}, -\frac{1}{2}}(\mathbf{r}_h^{\text{cr}}) &= \rho_0^h(\tilde{r}_h)Y_{0,0}(\Omega_h^{\text{cr}})\left|\frac{3}{2}, -\frac{1}{2}\right\rangle + \\ &+ \sqrt{\frac{2}{5}}\rho_2^h(\tilde{r}_h)\left[Y_{2,-2}(\Omega_h^{\text{cr}})\left|\frac{3}{2}, \frac{3}{2}\right\rangle - \right. \\ &\left. - Y_{2,1}(\Omega_h^{\text{cr}})\left|\frac{3}{2}, -\frac{3}{2}\right\rangle - \frac{1}{\sqrt{2}}Y_{2,0}(\Omega_h^{\text{cr}})\left|\frac{3}{2}, -\frac{1}{2}\right\rangle\right]. \quad (10) \end{aligned}$$

In expressions (7)–(10), $\rho_0^h(\tilde{r}_h)$ and $\rho_2^h(\tilde{r}_h)$ are the hole envelope size-quantized radial functions of the spherical and nonspherical, respectively, parts of the full hole wave function, the hole coordinates in the coordinate system $\{\tilde{X}, \tilde{Y}, \tilde{Z}\}$ are expressed using the radius vector $\tilde{\mathbf{r}}_h$, $r_h^{\text{cr}} \equiv \tilde{r}_h$, $|J, J_z\rangle$ are the on-site hole space-spin wave functions with the quantum number $J = 3/2$ of the total angular momentum (the effective spin) of the hole and the quantum number J_z of its projection on the axis Z_{cr} .

According to the standard sum rule for momenta, the functions $|J, J_z\rangle$ can be expressed as

$$|3/2, 3/2\rangle = (X^{\text{cr}} + iY^{\text{cr}})/\sqrt{2} \uparrow, \quad (11)$$

$$|3/2, -3/2\rangle = i(X^{\text{cr}} - iY^{\text{cr}})/\sqrt{2} \downarrow, \quad (12)$$

$$|3/2, 1/2\rangle = i[(X^{\text{cr}} + iY^{\text{cr}})\downarrow - 2Z^{\text{cr}}\uparrow]/\sqrt{6}, \quad (13)$$

$$|3/2, -1/2\rangle = [(X^{\text{cr}} - iY^{\text{cr}})\uparrow + 2Z^{\text{cr}}\downarrow]/\sqrt{6}, \quad (14)$$

where \uparrow and \downarrow are the hole spinors corresponding to the hole spin projections on the axis Z_{cr} equal to $\pm 1/2$; and X^{cr} , Y^{cr} , and Z^{cr} are the on-site hole spatial wave functions of the p -type in the crystal coordinate system $\{X_{\text{cr}}, Y_{\text{cr}}, Z_{\text{cr}}\}$.

In the case of the higher-energy triple degenerate states of bright excitons with $F = 1$ and $F_z = \pm 1, 0$, which are split off owing to the spin-spin electron-hole exchange interaction, the corresponding exciton size-quantized wave functions $\Psi_{\text{ex}}^{\text{el-h}}(F, F_z; \mathbf{r}_e^{\text{cr}}, \mathbf{r}_h^{\text{cr}})$ are as follows:

$$\begin{aligned} \Psi_{\text{ex}}^{\text{el-h}}(1, 1; \mathbf{r}_e^{\text{cr}}, \mathbf{r}_h^{\text{cr}}) &= \Psi_e^0(\mathbf{r}_e^{\text{cr}})\left[\frac{1}{2}\uparrow\Psi_h^{\frac{3}{2}, \frac{1}{2}}(\mathbf{r}_h^{\text{cr}}) - \right. \\ &\left. - \frac{\sqrt{3}}{2}i\downarrow\Psi_h^{\frac{3}{2}, \frac{3}{2}}(\mathbf{r}_h^{\text{cr}})\right], \quad (15) \end{aligned}$$

$$\begin{aligned} \Psi_{\text{ex}}^{\text{el-h}}(1, -1; \mathbf{r}_e^{\text{cr}}, \mathbf{r}_h^{\text{cr}}) &= \Psi_e^0(\mathbf{r}_e^{\text{cr}}) \times \\ &\times \left[\frac{\sqrt{3}}{2}\uparrow\Psi_h^{\frac{3}{2}, -\frac{3}{2}}(\mathbf{r}_h^{\text{cr}}) - \frac{1}{2}i\downarrow\Psi_h^{\frac{3}{2}, -\frac{1}{2}}(\mathbf{r}_h^{\text{cr}})\right], \quad (16) \end{aligned}$$

$$\Psi_{\text{ex}}^{\text{el-h}}(1, 0; \mathbf{r}_e^{\text{cr}}, \mathbf{r}_h^{\text{cr}}) = \frac{\Psi_e^0(\mathbf{r}_e^{\text{cr}})}{\sqrt{2}} \left[\uparrow \Psi_h^{\frac{3}{2}, -\frac{1}{2}}(\mathbf{r}_h^{\text{cr}}) - i \downarrow \Psi_h^{\frac{3}{2}, \frac{1}{2}}(\mathbf{r}_h^{\text{cr}}) \right]. \quad (17)$$

It should be noted that, in the seminal work by Efros *et al.* [4], the expressions for the exciton wave functions of dark excitons with $F = 2$ and $F_z = \pm 1$ contain an error. In the case of a spherical QD made up of a semiconductor of the cubic modification, those expressions should transform into expressions (3) and (4). However, this is not the case because, in work [4], the coefficients in front of the components in the corresponding wave functions are transposed. As a consequence, the wave functions of dark excitons with $F_z = \pm 1$ presented in work [4] are not orthogonal to the wave functions of bright excitons with $F_z = \pm 1$. Accordingly, the matrix elements of optical dark exciton transitions into/from those states, which were calculated in work [4] in the dipole approximation, differ from zero, unlike the zero matrix elements of the transition into/from the dark exciton states with $F_z = \pm 2$ and $F_z = 0$. Actually, they must be equal to zero in the dipole approximation as well. According to the results of our model, the radiation from all dark exciton states is emitted only in the form of spherical waves with the dipole and octupole components of the electric type and the quadrupole components of the magnetic type, and this emission is related only to the nonspherical part of the hole envelope wave function.

3. Transformation of Exciton Wave Functions at a Coordinate System Rotation

For further calculations of the QD + LF nanosystem, the exciton wave functions has to be written in the coordinate system $\{\tilde{X}, \tilde{Y}, \tilde{Z}\}$ with the origin O_2 located in the QD (Fig. 1). The orientation of the coordinate system $\{X_{\text{cr}}, Y_{\text{cr}}, Z_{\text{cr}}\}$ with respect to the system $\{\tilde{X}, \tilde{Y}, \tilde{Z}\}$ can be described conventionally, with the help of Euler angles $\{\Psi_e, \theta_e, \varphi_e\}$. In this work, all Euler angles are reckoned counterclockwise.

Note first that, in accordance with work [3], while finding the EM field emitted by the QD, we have to change from the electron-hole representation of exciton functions, $\Psi_{\text{ex}}^{\text{el-h}}(F, F_z; \mathbf{r}_e^{\text{cr}}, \mathbf{r}_h^{\text{cr}})$, to the electron-electron one, $\Psi_{\text{ex}}^{\text{el-el}}(F, F_z; \mathbf{r}_e^{\text{cr}}, \mathbf{r}_h^{\text{cr}})$, as was done in work [4]. This operation means a simple substitution of the spatial parts in the hole components of those

exciton functions by the complex conjugate ones and a substitution of the hole spinors \uparrow and \downarrow by the transposed electron spinors \uparrow^T and \downarrow^T , respectively. As a result, in the initial crystal coordinate system, the exciton wave functions $\Psi_{\text{ex}}^{\text{el-el}}(F, F_z; \mathbf{r}_e^{\text{cr}}, \mathbf{r}_h^{\text{cr}})$ will include the spinor products $\uparrow\uparrow^T$ and $\downarrow\downarrow^T$, which are scalars and equal 1, and spinor products $\uparrow\downarrow^T$ and $\downarrow\uparrow^T$ equal to zero. Therefore, first, only those components will survive in the expressions for EM fields, which correspond to nonzero spinor products. Second, the products $\uparrow\uparrow^T$ and $\downarrow\downarrow^T$ equal 1 in the coordinate system $\{\tilde{X}, \tilde{Y}, \tilde{Z}\}$ as well.

As for the angular envelope functions $Y_{2,\mu}(\Omega^{\text{cr}})$ in Eqs. (7)–(10), according to work [7], they can be expanded in a series of the spherical harmonics $Y_{2,m}(\tilde{\Omega})$ in the coordinate system $\{\tilde{X}, \tilde{Y}, \tilde{Z}\}$ as follows:

$$Y_{2,\mu}(\theta_{\text{cr}}, \varphi_{\text{cr}}) = \sum_{m=-2}^2 C_{\mu,m} Y_{2,m}(\tilde{\theta}, \tilde{\varphi}). \quad (18)$$

The expansion coefficients $C_{\mu,m}$ can be found with the use of the following expressions for the spherical harmonics $Y_{2,\mu}(\Omega^{\text{cr}})$:

$$Y_{2,\pm 2}(\Omega^{\text{cr}}) = \sqrt{15/(32\pi)}(x_{\text{cr}} \pm iy_{\text{cr}})^2,$$

$$Y_{2,\pm 1}(\Omega^{\text{cr}}) = \mp \sqrt{15/(8\pi)}(x_{\text{cr}} \pm iy_{\text{cr}})z_{\text{cr}},$$

$$Y_{2,0}(\Omega^{\text{cr}}) = \sqrt{5/(16\pi)}(2z_{\text{cr}}^2 - x_{\text{cr}}^2 - y_{\text{cr}}^2),$$

where x_{cr} , y_{cr} , and z_{cr} are the coordinates of the unit vector oriented in the direction given by the angles θ_{cr} and φ_{cr} in the crystal coordinate system, i.e. $x_{\text{cr}} = \sin \theta_{\text{cr}} \cos \varphi_{\text{cr}}$, $y_{\text{cr}} = \sin \theta_{\text{cr}} \sin \varphi_{\text{cr}}$, and $z_{\text{cr}} = \cos \theta_{\text{cr}}$. Expressing the coordinates x_{cr} , y_{cr} and, z_{cr} of the unit vector in terms of Euler angles and the coordinates of this vector in the coordinate system $\{\tilde{X}, \tilde{Y}, \tilde{Z}\}$, i.e. in terms of $\tilde{x} = \sin \tilde{\theta} \cos \tilde{\varphi}$, $\tilde{y} = \sin \tilde{\theta} \sin \tilde{\varphi}$, and $\tilde{z} = \cos \tilde{\theta}$, multiplying formula (18) by $Y_{2,m}^*(\tilde{\theta}, \tilde{\varphi})$, and integrating the result over the angular variables $\tilde{\theta}$ and $\tilde{\varphi}$, we obtain expressions for the coefficients $C_{\mu,m}$ as functions of the Euler angles. They are quoted in Appendix 1.

At last, while calculating the contribution of point (on-site) emitting dipoles to the total electromagnetic field of a QD, the matrix elements of on-site dipole moments are expressed in the form $\langle S | \mathbf{e} \mathbf{r}_i | X^{\text{cr}} \rangle = p \mathbf{n}_1$, $\langle S | \mathbf{e} \mathbf{r}_i | Y^{\text{cr}} \rangle = p \mathbf{n}_2$, and $\langle S | \mathbf{e} \mathbf{r}_i | Z^{\text{cr}} \rangle = p \mathbf{n}_3$, where \mathbf{r}_i is the electron coordinate in the elementary

cell corresponding to that or another crystal site, p the magnitude of on-site dipole moment (owing to the cubic crystal symmetry, it is identical for all three directions), \mathbf{n}_1 , \mathbf{n}_2 , and \mathbf{n}_3 are the unit vectors of the crystal coordinate system. In the coordinate system $\{\tilde{X}, \tilde{Y}, \tilde{Z}\}$, those unit vectors at the site with the coordinate $\tilde{\mathbf{r}}_d$ (see Fig. 1) can be expressed in the form [5]

$$\begin{aligned} \mathbf{n}_\alpha(\tilde{\mathbf{r}}_d) &= \sqrt{2\pi/3} \times \\ &\times \left\{ n_\alpha^x \nabla_{\tilde{\mathbf{r}}_d} [\tilde{r}_d \{Y_{1,-1}(\tilde{\Omega}_d) - Y_{1,1}(\tilde{\Omega}_d)\}] + \right. \\ &+ i n_\alpha^y \nabla_{\tilde{\mathbf{r}}_d} [\tilde{r}_d \{Y_{1,-1}(\tilde{\Omega}_d) + Y_{1,1}(\tilde{\Omega}_d)\}] + \\ &\left. + \sqrt{2} n_\alpha^z \nabla_{\tilde{\mathbf{r}}_d} [\tilde{r}_d Y_{1,0}(\tilde{\Omega}_d)] \right\}, \end{aligned} \quad (19)$$

where n_α^x , n_α^y , and n_α^z are the components of the vector \mathbf{n}_α in the coordinate system $\{\tilde{X}, \tilde{Y}, \tilde{Z}\}$. According to the on-site hole wave functions (11)–(14), the following combinations of those components are relevant to our calculations:

$$n_1^x \pm i n_2^x = \exp(\mp i \varphi_e) [\cos \Psi_e \mp i \cos \theta_e \sin \Psi_e], \quad (20)$$

$$n_1^y \pm i n_2^y = \exp(\mp i \varphi_e) [\sin \Psi_e \pm i \cos \theta_e \cos \Psi_e], \quad (21)$$

$$n_1^z \pm i n_2^z = \pm i \exp(\mp i \varphi_e) \sin \theta_e, \quad (22)$$

$$n_3^x = \sin \theta_e \sin \Psi_e, \quad n_3^y = -\sin \theta_e \cos \Psi_e, \quad (23)$$

$$n_3^z = \cos \theta_e. \quad (24)$$

4. Electromagnetic Fields of QD Excitonic Emission

While calculating the EM field emitted by the fivefold degenerate state of dark excitons in a QD characterized by the quantum number $F = 2$ of the total exciton angular momentum, the following effective wave function has to be used:

$$\begin{aligned} \Psi_{\text{ex},2}(\tilde{\mathbf{r}}_e, \tilde{\mathbf{r}}_h) &= \frac{1}{\sqrt{5}} [a_L \Psi_{\text{ex}}^{\text{el-el}}(2, 0; \tilde{\mathbf{r}}_e, \tilde{\mathbf{r}}_h) + \\ &+ b_L \Psi_{\text{ex}}^{\text{el-el}}(2, 1; \tilde{\mathbf{r}}_e, \tilde{\mathbf{r}}_h) + c_L \Psi_{\text{ex}}^{\text{el-el}}(2, -1; \tilde{\mathbf{r}}_e, \tilde{\mathbf{r}}_h) + \\ &+ d_L \Psi_{\text{ex}}^{\text{el-el}}(2, 2; \tilde{\mathbf{r}}_e, \tilde{\mathbf{r}}_h) + f_L \Psi_{\text{ex}}^{\text{el-el}}(2, -2; \tilde{\mathbf{r}}_e, \tilde{\mathbf{r}}_h)], \end{aligned} \quad (25)$$

where a_L , b_L , c_L , d_L , and f_L are arbitrary phase factors. Such a form for the effective wave function is associated with an identical population probability for

each of five degenerate states of dark excitons in the case of an external excitation. The very presence of arbitrary phase factors stems from the noncoherent exciton behavior in those states. Accordingly, while calculating the EM field emitted by the triple degenerate state of bright excitons in a QD characterized by the quantum number $F = 1$ of the total exciton angular momentum, the effective wave function looks like

$$\begin{aligned} \Psi_{\text{ex},1}(\tilde{\mathbf{r}}_e, \tilde{\mathbf{r}}_h) &= \frac{1}{\sqrt{3}} [a_U \Psi_{\text{ex}}^{\text{el-el}}(1, 0; \tilde{\mathbf{r}}_e, \tilde{\mathbf{r}}_h) + \\ &+ b_U \Psi_{\text{ex}}^{\text{el-el}}(1, 1; \tilde{\mathbf{r}}_e, \tilde{\mathbf{r}}_h) + c_U \Psi_{\text{ex}}^{\text{el-el}}(1, -1; \tilde{\mathbf{r}}_e, \tilde{\mathbf{r}}_h)], \end{aligned} \quad (26)$$

where a_U , b_U , and c_U are also arbitrary phase factors.

According to work [3], the electric field, which is generated by the emission of all on-site dipoles in the QD and is associated with the exciton state characterized by the quantum number F of the total angular momentum, at the internal QD surface must have the form

$$\begin{aligned} \mathbf{E}_{\text{QD},2}^i(\tilde{\mathbf{r}}; F) &= \sum_{l,m} \left\{ \frac{i}{k_0 \varepsilon_2} \tilde{a}_{2,E}^{i,F}(l, m) \times \right. \\ &\times [\nabla_{\tilde{\mathbf{r}}} \times h_l(k_2 \tilde{r}) \mathbf{X}_{l,m}(\tilde{\Omega})] + \\ &\left. + \tilde{a}_{2,M}^{i,F}(l, m) h_l(k_2 \tilde{r}) \mathbf{X}_{l,m}(\tilde{\Omega}) \right\}, \end{aligned} \quad (27)$$

where $\tilde{r} = R_2$, subscript 2 in $\mathbf{E}_{\text{QD},2}^i$ means that this is the field at the internal side of the QD interface (see Fig. 1), $k_0 = \omega/c$, c is the light velocity, $k_2 = \sqrt{\varepsilon_2} k_0$, $\tilde{a}_{2,E}^{i,F}(l, m)$ and $\tilde{a}_{2,M}^{i,F}(l, m)$ are coefficients in the multipole expansions of the electric field (of the electric and magnetic types, respectively) emitted by the exciton state with the quantum number F of the total angular momentum, ε_2 is the background dielectric constant of a semiconductor in the radiation emission frequency interval (in the case of CdTe, $\varepsilon_2 \approx 13$ in the interval $\hbar\omega = 1.5 \div 3.0$ eV [8]), $\mathbf{X}_{l,m}(\tilde{\Omega})$ are the normalized vector spherical harmonics [9], and $h_l(x)$ is the spherical Hankel function of the first kind.

The dipole moment of the site with the coordinate $\tilde{\mathbf{r}}_d$ can be written as the expansion

$$\begin{aligned} \langle 0 | e \tilde{\mathbf{r}}_i | \Psi_{\text{ex},F}(\tilde{\mathbf{r}}_e, \tilde{\mathbf{r}}_h) \rangle_{\tilde{\mathbf{r}}_d} &= p [\mathbf{n}_1 \Psi_{\text{ex},F}^{(1)}(\tilde{\mathbf{r}}_d, \tilde{\mathbf{r}}_d) + \\ &+ \mathbf{n}_2 \Psi_{\text{ex},F}^{(2)}(\tilde{\mathbf{r}}_d, \tilde{\mathbf{r}}_d) + \mathbf{n}_3 \Psi_{\text{ex},F}^{(3)}(\tilde{\mathbf{r}}_d, \tilde{\mathbf{r}}_d)], \end{aligned} \quad (28)$$

where $|0\rangle = \delta(\tilde{\mathbf{r}}_e - \tilde{\mathbf{r}}_h)$, and the functions $\Psi_{\text{ex},F}^{(j)}(\tilde{\mathbf{r}}_d, \tilde{\mathbf{r}}_d)$ are coefficients at the on-site functions $X^{\text{cr}}(j = 1)$,

$Y^{\text{cr}}(j=2)$, and $Z^{\text{cr}}(j=3)$ in the full wave function $\Psi_{\text{ex},F}(\tilde{\mathbf{r}}_d, \tilde{\mathbf{r}}_d)$. Hence, this dipole moment is composed of the dipole moments of three point dipoles located at the site $\tilde{\mathbf{r}}_d$ and oriented along the unit vectors of the intrinsic (crystal) coordinate system \mathbf{n}_1 , \mathbf{n}_2 , and \mathbf{n}_3 .

The contribution to the electric field (27) given by a point dipole with moment p located in a QD at the point $\tilde{\mathbf{r}}_d$ and oriented along \mathbf{n}_α is expressed by the formula [3]

$$\begin{aligned} \mathbf{E}_{d,2}^i(\tilde{\mathbf{r}}, \tilde{\mathbf{r}}_d; \mathbf{n}_\alpha) &= \sum_{l=1}^{\infty} \sum_{m=-l}^l \left\{ \frac{i}{k_0 \varepsilon_2} \tilde{a}_{d,E}^{\gt}(l, m) \times \right. \\ &\times [\nabla_{\tilde{\mathbf{r}}} \times h_l(k_2 \tilde{r}) \mathbf{X}_{l,m}(\tilde{\Omega})] + \\ &\left. + \tilde{a}_{d,M}^{\gt}(l, m) h_l(k_2 \tilde{r}) \mathbf{X}_{l,m}(\tilde{\Omega}) \right\}, \end{aligned} \quad (29)$$

where

$$\begin{aligned} \tilde{a}_{d,M}^{\gt}(l, m) &= 4\pi i p k_2 k_0^2 j_l(k_2 \tilde{r}_d) \mathbf{n}_\alpha \cdot \mathbf{X}_{l,m}^*(\tilde{\Omega}_d), \\ \tilde{a}_{d,E}^{\gt}(l, m) &= 4\pi p k_2 k_0 \mathbf{n}_\alpha \cdot [\nabla_{\tilde{\mathbf{r}}_d} \times j_l(k_2 \tilde{r}_d) \mathbf{X}_{l,m}^*(\tilde{\Omega}_d)], \end{aligned}$$

and $j_l(x)$ is the spherical Bessel function.

The total electric field (27) emitted by the QD and the corresponding multipole coefficients $\tilde{a}_{2,E}^{i,F}(l, m)$ and $\tilde{a}_{2,M}^{i,F}(l, m)$ can be obtained by integrating contributions (29) of all point (on-site) dipoles over the QD volume on the basis of the effective wave functions (25) and (26):

$$\begin{aligned} \mathbf{E}_{QD,2}^i(\tilde{\mathbf{r}}; F) &= \sum_{\alpha=1,2,3} \int_{\text{QD}} \Psi_{\text{ex},F}^{(\alpha)}(\tilde{\mathbf{r}}_d, \tilde{\mathbf{r}}_d) \times \\ &\times \mathbf{E}_{d,2}^i(\tilde{\mathbf{r}}, \tilde{\mathbf{r}}_d; \mathbf{n}_\alpha) d^3 \tilde{r}_d. \end{aligned} \quad (30)$$

Taking into account that (see, e.g., work [10])

$$\begin{aligned} \int_{-1}^1 (1-x^2)^{\lambda-1} P_l^m(x) dx &= \pi 2^m \times \\ &\times \frac{\Gamma(\lambda + \frac{m}{2}) \Gamma(\lambda - \frac{m}{2})}{\Gamma(\lambda + \frac{l+1}{2}) \Gamma(\lambda - \frac{l}{2}) \Gamma(1 + \frac{l-m}{2}) \Gamma(\frac{1-l-m}{2})}, \end{aligned} \quad (31)$$

$$\begin{aligned} \int_0^1 x^\sigma (1-x^2)^{m/2} P_l^m(x) dx &= \frac{(-1)^m}{2^{m+1}} \times \\ &\times \frac{\Gamma(\frac{1+\sigma}{2}) \Gamma(1 + \frac{\sigma}{2}) \Gamma(1+m+l)}{\Gamma(1 + \frac{\sigma+m-l}{2}) \Gamma(\frac{3+\sigma+m+l}{2}) \Gamma(1-m+l)}, \end{aligned} \quad (32)$$

where $P_l^m(x)$ are the associated Legendre polynomials, we obtain that only the multipoles of the magnetic type with $l=2$ and the multipoles of the electric type with $l=1$ and 3 survive after the integration from an infinite number of multipoles (29) in the integrand of expression (30). Hence, it is possible to determine all multipole coefficients $\tilde{a}_{2,E}^{i,F}(l, m)$ and $\tilde{a}_{2,M}^{i,F}(l, m)$ in expansion (27) of the electric field of the QD excitonic emission at the internal QD boundary as functions of the Euler angles. All other fields, including ones reflected from the metal NP and the field in the NP, can be determined, by using the formulas presented in work [3].

5. Energies of Exciton Transitions and Radial Wave Functions of an Electron and a Hole

To calculate the emission characteristics of the nanosystem QD + NP, it is necessary to determine the exciton transition energy E_x in the QD (i.e. the radiation frequency $\omega = E_x/\hbar$ in formula (27)) as a function of the QD size. Unlike works [4], [11], and others, where the approximation of infinitely high barriers for electrons and holes was used (the corresponding values of size-quantized energies turn out substantially overestimated), the calculations in this work are carried out for a more realistic case of barriers with finite heights, namely, for the case where a CdTe QD and a metal NP are located in the SiO₂ matrix. Generally speaking, this choice is related to the fact that all SiO₂ parameters required for calculations, as well as the discontinuities of the valence and conduction bands across the CdTe/SiO₂ interface, are known or could be calculated. In addition, SiO₂ is used in real structures as an intermediate layer and a coating of CdTe QDs and metal NPs (see, e.g., works [12–15]).

The envelope wave functions and the energies of exciton states in a separate QD are determined from the Schrödinger equation

$$\begin{aligned} &[\hat{H}_e + \hat{H}_h + \hat{H}_{\text{exch}} + U_e(r_e^{\text{cr}}) + U_h(r_h^{\text{cr}}) + \\ &+ U_s(r_e^{\text{cr}}) + U_s(r_h^{\text{cr}}) + U_{eh}(\mathbf{r}_e^{\text{cr}}, \mathbf{r}_h^{\text{cr}})] \times \\ &\times \Psi_{\text{ex},F}(\mathbf{r}_e^{\text{cr}}, \mathbf{r}_h^{\text{cr}}) = (E_{x,F} - E_g) \Psi_{\text{ex},F}(\mathbf{r}_e^{\text{cr}}, \mathbf{r}_h^{\text{cr}}), \end{aligned} \quad (33)$$

where E_g is the energy gap width in the QD bulk material (in the case of CdTe, $E_g = 1.475$ eV at $T =$

= 300 K [8]), \hat{H}_e and \hat{H}_h are the electron and hole, respectively, kinetic energy operators in the Luttinger–Kohn multiband model,

$$\hat{H}_{\text{exch}} = -(\hbar\omega_{\text{ST}}/12) a_{\text{ex}}^3 \delta(\mathbf{r}_e^{\text{cr}} - \mathbf{r}_h^{\text{cr}}) (\boldsymbol{\sigma} \cdot \mathbf{J})$$

is the operator of electron-hole exchange interaction [4], $\hbar\omega_{\text{ST}}$ the singlet-triplet splitting in the bulk semiconductor (for CdTe, $\hbar\omega_{\text{ST}} = 0.04$ meV), a_{ex} the exciton Bohr radius (for CdTe, $a_{\text{ex}} \approx 6.5$ nm), $\boldsymbol{\sigma}$ are the electron Pauli matrices for particles with spin 1/2, and \mathbf{J} the hole matrices for particles with spin 3/2. The potential energies $U_s(r_e^{\text{cr}})$ and $U_s(r_h^{\text{cr}})$ describe the self-action of an electron and a hole, respectively, in the field of image charge forces that emerge owing to the polarization of the heterointerface in the QD. The potential energies $U_e(r_e^{\text{cr}})$ and $U_h(r_h^{\text{cr}})$ describe the energy wells for electrons and holes, respectively, which are formed as a result of discontinuities of the conduction and valence bands at the heterointerface; $U_{e(h)}(r) = 0$ if $r < R_2$, and $U_{e(h)}(r) = U_{c(v)}$ if $r > R_2$, where R_2 is the QD radius; the valence band discontinuity at the heterointerface CdTe/SiO₂ amounts to $U_v = 4.7$ eV [16], and that of the conduction band to $U_c = 2.92$ eV (taking into account that the energy gap width in SiO₂ amounts to 9.1 eV). The potential energy $U_{eh}(\mathbf{r}_e^{\text{cr}}, \mathbf{r}_h^{\text{cr}})$ describes the electron-hole Coulomb interaction (both direct and indirect, i.e. through the corresponding polarization of the heterointerface). It can be determined by solving the Poisson equation

$$\nabla_{\mathbf{r}} \cdot [\varepsilon(r) \nabla_{\mathbf{r}} U(\mathbf{r}, \mathbf{r}')] = 4\pi e^2 \delta(\mathbf{r} - \mathbf{r}'),$$

where $\varepsilon(r) = \varepsilon_2^0$ if $r < R_2$ and $\varepsilon(r) = \varepsilon_3^0$ if $r > R_2$, ε_2^0 is the low-frequency (static) dielectric constant of a QD material (for CdTe, $\varepsilon_2^0 = 10.4$ [8]), ε_3^0 the low-frequency dielectric constant of the matrix material (for SiO₂, $\varepsilon_3^0 = 3.9$ [8]), and e the electron charge. The expressions for the potential self-action, $U_s(r)$, and interaction, $U_{eh}(\mathbf{r}, \mathbf{r}')$, energies can be found, e.g., in work [17] in a form convenient for quantum-mechanical calculations.

The radial electron wave function $\rho_0^e(\tilde{r}_e)$ of the ground electron state in a QD ($\tilde{r}_e \equiv r_e^{\text{cr}}$), which is the eigenfunction of the kinetic energy operator \hat{H}_e , has the following form in the finite-barrier case:

$$\rho_0^e(\tilde{r}_e) = C_e \{ \theta(R_2 - \tilde{r}_e) j_0(k_e \tilde{r}_e) + \theta(\tilde{r}_e - R_2) \times \\ \times k_0(\lambda_e \tilde{r}_e) [j_0(k_e R_2)/k_0(\lambda_e R_2)] \}, \quad (34)$$

where $j_0(x)$ is the spherical Bessel function of the zeroth order, $k_0(x) = \exp(x)/x$ is the modified spherical Hankel function of the zeroth order, $k_e = \sqrt{2m_{e,2}E_e}/\hbar$, $\lambda_e = \sqrt{2m_{e,3}(U_c - E_e)}/\hbar$, $m_{e,2}$ is the effective electron mass in the QD (for CdTe, $m_{e,2} = 0.095m_0$ [8]), and $m_{e,3}$ the effective electron mass in the surrounding matrix (for SiO₂, $m_{e,3} = 0.5m_0$ [18]). The size-quantized electron energy E_e is determined from the condition of a nontrivial solution for boundary conditions in the form of the continuity of the wave function and its flux across the QD/matrix interface, and the normalization constant C_e from the normalization condition $\int_0^\infty [\rho_0^e(\tilde{r}_e)]^2 \tilde{r}_e^2 d\tilde{r}_e = 1$.

The radial hole wave functions $\rho_0^h(\tilde{r}_h)$ and $\rho_2^h(\tilde{r}_h)$ of the ground hole state in a QD ($\tilde{r}_h \equiv r_h^{\text{cr}}$) have the following form in the case of finite barrier:

$$\rho_0^h(\tilde{r}_h) = \theta(R_2 - \tilde{r}_h) [A j_0(k_{hh} \tilde{r}_h) + B j_0(k_{lh} \tilde{r}_h)] + \\ + \theta(\tilde{r}_h - R_2) [C k_0(\lambda_{hh} \tilde{r}_h) + D k_0(\lambda_{lh} \tilde{r}_h)], \quad (35)$$

$$\rho_2^h(\tilde{r}_h) = \theta(R_2 - \tilde{r}_h) [A j_2(k_{hh} \tilde{r}_h) - B j_2(k_{lh} \tilde{r}_h)] + \\ + \theta(\tilde{r}_h - R_2) [C k_2(\lambda_{hh} \tilde{r}_h) - D k_2(\lambda_{lh} \tilde{r}_h)], \quad (36)$$

where $j_2(x)$ is the spherical Bessel function of the second order, $k_2(x) = \exp(-x)(1/x + 3/x^2 + 3/x^3)$ is the modified spherical Hankel function of the second order, $k_{hh} = \sqrt{2m_{hh,2}E_h}/\hbar$, $k_{lh} = \sqrt{2m_{lh,2}E_h}/\hbar$, $\lambda_{hh} = \sqrt{2m_{hh,3}(U_v - E_h)}/\hbar$, $\lambda_{lh} = \sqrt{2m_{lh,3}(U_v - E_h)}/\hbar$, $m_{hh,2}$ and $m_{lh,2}$ are the effective masses of heavy and light, respectively, holes in the QD (for CdTe, $m_{hh,2} = 0.81m_0$ and $m_{lh,2} = 0.12m_0$ [8]), and $m_{hh,3}$ and $m_{lh,3}$ the effective masses of heavy and light holes in the matrix (for SiO₂, $m_{hh,3} = m_{lh,3} = 0.6m_0$ [19]). The size-quantized hole energy is also determined from the condition of a nontrivial solution for boundary conditions in the form of the continuity of the wave function and its flux across the QD/matrix interface, the constants A , B , C , and D are determined from those boundary conditions and the normalization one

$$\int_0^\infty \{ [\rho_0^h(\tilde{r}_h)]^2 + [\rho_2^h(\tilde{r}_h)]^2 \} \tilde{r}_h^2 d\tilde{r}_h = 1.$$

In Fig. 2, the dependences of the exciton transition energy E_x in the CdTe QD on the QD radius R_2 are depicted. They have been obtained neglecting the exchange interaction operator \hat{H}_{exch} in the Schrödinger equation (33).

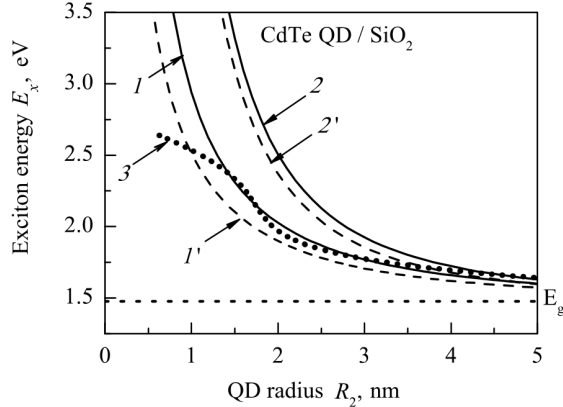


Fig. 2. Dependences of the main exciton transition energy E_x on the QD radius for the CdTe QD. Curves 1 and 1' correspond to a finite CdTe/SiO₂ barrier, and 2 and 2' to an infinitely high one. Curves 1 and 2 were calculated taking the mixing of heavy and light hole states into account, and curves 1' and 2' with only heavy hole state account. Curve 3 is the empirical dependence of the energy of the first absorption peak on the CdTe QD radius [20]

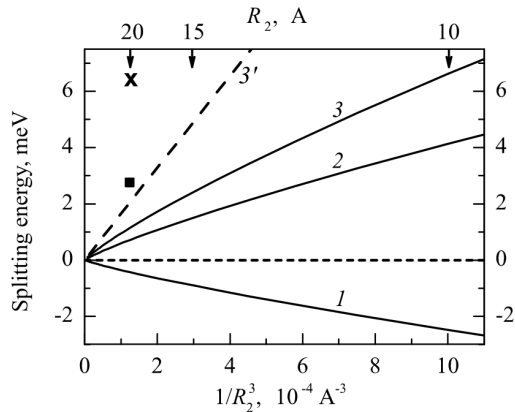


Fig. 3. Dependences of the energies $E_{x,F} - E_x$ on the CdTe QD radius. Curve 1 corresponds to the states of dark excitons with the quantum number $F = 2$ of the total angular momentum, curve 2 to states of bright excitons with $F = 1$. Curve 3 illustrates the dependence of the total splitting $\Delta = E_{x,1} - E_{x,2}$. The dashed curve 3' is the dependence of the total splitting in the case of infinitely high barriers for electrons and holes. The symbol \times marks the value of total splitting in the CdTe QD with $R_2 = 2$ nm obtained in accordance with the calculations by Efros *et al.* [4]; and the symbol \blacksquare , in accordance with the calculations by Blokland *et al.* [11]

Figure 3 illustrates the calculated dependences of the energies of dark and bright excitons (reckoned from the exciton transition energies E_x shown in Fig. 2) on the CdTe QD radius.

640

6. Energies of Plasmons in a Metal NP

The interaction of the QD excitonic emission with plasma oscillations in the NP and the excitonic emission enhancement owing to this interaction become maximal under conditions close to the resonance between the excitonic emission energy and the energy of plasma oscillations. Specific calculations were carried out for gold and silver NPs, whose dielectric functions in the optical spectral range can be written in the form [21, 22]

$$\varepsilon_1^{T(L)}(\omega, k) = 1 + \varepsilon_{ib}(\omega) + \varepsilon_{pl}^{T(L)}(\omega, k), \quad (37)$$

where the second term on the right-hand side is associated with interband electron transitions (i.e. with bound electrons) and the third one,

$$\varepsilon_{pl}^{T(L)}(\omega, k) = -\frac{\omega_{pl}^2}{\omega[\omega + i(\Gamma + Av_F/R_1)] - \beta_{T(L)}^2 k^2}, \quad (38)$$

with electron transitions in the conduction band (i.e. with free electrons). The indices T and L denote the transverse and longitudinal, respectively, components of the dielectric constant. In gold or silver, the Fermi velocity $v_F \approx 1.4 \times 10^8$ cm/s, $\beta_L = \sqrt{3/5}v_F$, $\beta_T = 0$, the damping constant in the bulk material $\Gamma = v_F/l_f$, l_f is the mean free path of electrons, the constant A falls within the interval of 0.1–0.7 depending on the mechanism of electron scattering by NP walls and other factors [21] (in this work, we put $A = 0.5$), $\omega_{pl} = \sqrt{4\pi ne^2/m^*}$ is the plasma frequency of the corresponding material (for gold, $\hbar\omega_{pl} = 8.56$ eV and $\hbar\Gamma = 73$ meV [23]; for silver, $\hbar\omega_{pl} = 9.1$ eV and $\hbar\Gamma = 18$ meV [24]). In the case of gold, the interband transitions are taken into account on the basis of a model presented in work [23] with interband transition energies $\hbar\omega_1 = 2.65$ eV and $\hbar\omega_2 = 3.75$ eV. In the case of silver, the generalized Drude model is used with the background dielectric constant $\varepsilon_\infty = 1 + \varepsilon_{ib} = 3.71$ [24]. The frequency dependences of the real and imaginary parts of the dielectric constants calculated for massive gold and silver on the basis of models [23] and [24] agree well with experimental data [25] in the relevant frequency interval.

The energy of interface plasmon oscillations in metal NPs can be determined in the framework of the scattering problem as poles of the reflection coefficients $V_{E,33}^{NP}$ for the electromagnetic radiation incident on a NP calculated in our previous work [3]. In

Figs. 4 and 5, the dependences of the energies of interface plasmons of various orders on the radius of a gold or silver, respectively, NP in the SiO₂ matrix characterized by the high-frequency dielectric constant $\varepsilon_3 \approx 2.37 \div 2.45$ in the energy interval 1.6–3 eV [26] are shown.

7. Calculation of Excitonic Emission Power in the Nanosystem “Semiconductor QD + Metal NP”

In Section 4, we have calculated the EMFs generated on the internal side of the QD surface due to the excitonic emission. All other fields in a QD + NP nanosystem can be found using formulae of our previous work [3]. Now, we can calculate the emission power for both an isolated QD and a nanosystem QD + NP in whole. According to work [9], the power emitted by an isolated semiconductor QD and averaged over the period $T = 2\pi/\omega$ looks like

$$\bar{P}_{\text{QD}}^{(F)} = \frac{\omega}{8\pi k_3^3} \sum_{l,m} [|\tilde{a}_{3,E}^{t,F}(l,m)|^2 + \varepsilon_3 |\tilde{a}_{3,M}^{t,F}(l,m)|^2], \quad (39)$$

where the coefficients $\tilde{a}_{3,E}^{t,F}(l,m)$ and $\tilde{a}_{3,M}^{t,F}(l,m)$ of the multipole expansion of the EM field outside the QD are connected with the calculated coefficients $\tilde{a}_{2,E}^{i,F}(l,m)$ and $\tilde{a}_{2,M}^{i,F}(l,m)$ of EM fields at the internal QD boundary by means of the EM field transmission coefficients $V_{E,23}^{\text{QD}}(l)$ and $V_{M,23}^{\text{QD}}(l)$, respectively [3].

As a result, in the case of emission from the higher bright exciton levels with $F = 1$, the following expression is obtained:

$$\begin{aligned} \bar{P}_{\text{QD}}^{(1)} &= \frac{\omega |p|^2 k_0^3}{108} \left(\frac{\varepsilon_2}{\varepsilon_3}\right)^{3/2} \left[\sqrt{\varepsilon_2} |V_{E,23}^{\text{QD}}(1)|^2 I_0^2 \times \right. \\ &\times \left(24 - 8 \frac{I_2}{I_0} + \frac{13}{2} \frac{I_2^2}{I_0^2} \right) + \frac{192}{7} \sqrt{\varepsilon_2} |V_{E,23}^{\text{QD}}(3)|^2 I_2^2 + \\ &\left. + \frac{3234}{125} \frac{\varepsilon_3}{\sqrt{\varepsilon_2}} |V_{M,23}^{\text{QD}}(2)|^2 I_2^2 \right], \quad (40) \end{aligned}$$

where

$$I_0 = \int_0^{R_2} \rho_0^e(\tilde{r}) \rho_0^h(\tilde{r}) j_0(k_2 \tilde{r}) \tilde{r}^2 d\tilde{r},$$

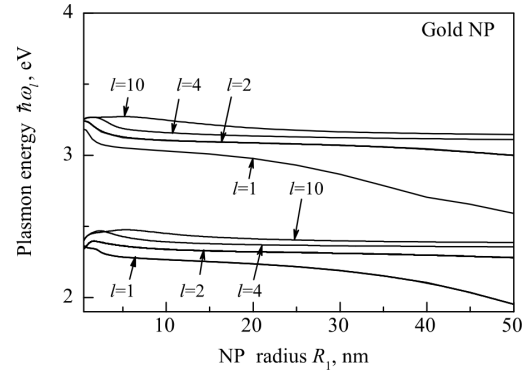


Fig. 4. Dependences of the energy of interface plasmons in a gold NP on the NP radius for various orbital numbers l

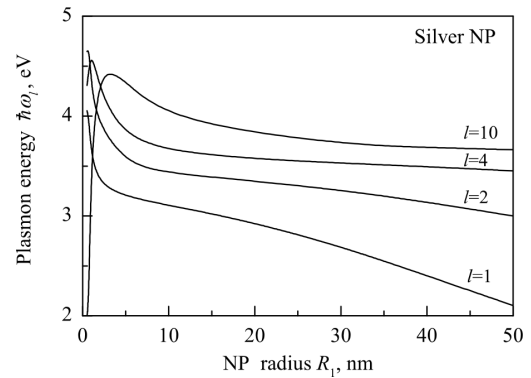


Fig. 5. The same as in Fig. 4, but for silver NPs

$$I_2 = \int_0^{R_2} \rho_0^e(\tilde{r}) \rho_2^h(\tilde{r}) j_2(k_2 \tilde{r}) \tilde{r}^2 d\tilde{r}.$$

In the case of emission from the lower levels of dark excitons with $F = 2$,

$$\begin{aligned} \bar{P}_{\text{QD}}^{(2)} &= \frac{\omega |p|^2 k_0^3}{450} \left(\frac{\varepsilon_2}{\varepsilon_3}\right)^{3/2} I_2^2 \left[6 \sqrt{\varepsilon_2} |V_{E,23}^{\text{QD}}(1)|^2 + \right. \\ &\left. + \frac{128}{7} \sqrt{\varepsilon_2} |V_{E,23}^{\text{QD}}(3)|^2 + \frac{392}{5} \frac{\varepsilon_3}{\sqrt{\varepsilon_2}} |V_{M,23}^{\text{QD}}(2)|^2 \right]. \quad (41) \end{aligned}$$

From formulas (40) and (41), one can see that the power emitted by an isolated semiconductor QD does not depend on the Euler angles, which is evident from the physical reason. This fact confirms the correctness of the results obtained for the electric fields.

In the presence of a metal NP in a vicinity of the semiconductor QD, the field in the wave zone is a sum of the EM field emitted by the QD itself and the

fields formed as a result of the multiple field scattering between the QD and the NP. The field emitted by the QD contains only the multipole components with $l = 1, 2$, and 3 . However, in the course of scattering of this field between the QD and the NP, the other multipole components of higher orders l' emerge [3]. The components with larger l' -values correspond to the less contributions to the total field. Therefore, we may confine the consideration to a finite number of multipoles. In the further consideration, for the sake of brevity, we use the notation of work [3], including that for the coefficients of reflection and transmission of the EM field at the heterointerfaces matrix/NP and matrix/QD.

Let the number k denote the maximum order of multipoles that are taken into account in the scattering. The matrix $\mathbf{N}^{(m)}$ is formed as a sum of the powers of matrices for a single scattering of the EM field by the QD [3]:

$$\mathbf{N}^{(m)} = \mathbf{I} + \boldsymbol{\xi}_m + \boldsymbol{\xi}_m^2 + \dots = (\mathbf{I} - \boldsymbol{\xi}_m)^{-1}. \quad (42)$$

This is a $2k \times 2k$ -matrix describing the multiple EM field scattering by the QD. Let us also define the $2k \times 2k$ -matrix $\mathbf{M}^{(m)} = \mathbf{Z}_m \mathbf{N}^{(m)}$ with regard for the multiple scattering of an EM field by the metal NP (the $2k \times 2k$ -matrix \mathbf{Z}_m is defined in work [3]). Let us also introduce the following quantities, in which the elements of matrices $\mathbf{M}^{(m)}$ and $\mathbf{N}^{(m)}$ are used:

$$\begin{aligned} B_{l,n}^{(m)} &= |V_{E,33}^{\text{NP}}(l) M_{k+l,n}^{(m)} + N_{k+l,n}^{(m)}|^2 + \\ &+ \varepsilon_3 |V_{M,33}^{\text{NP}}(l) M_{l,n}^{(m)} + N_{l,n}^{(m)}|^2, \quad (43) \\ C_{l,n,j}^{(m)} &= [V_{E,33}^{\text{NP}}(l) M_{k+l,n}^{(m)} + N_{k+l,n}^{(m)}] \times \\ &\times [V_{E,33}^{\text{NP}}(l) M_{k+l,j}^{(m)} + N_{k+l,j}^{(m)}]^* + \\ &+ \varepsilon_3 [V_{M,33}^{\text{NP}}(l) M_{l,n}^{(m)} + N_{l,n}^{(m)}] \times \\ &\times [V_{M,33}^{\text{NP}}(l) M_{l,j}^{(m)} + N_{l,j}^{(m)}]^*. \quad (44) \end{aligned}$$

The expressions obtained with the use of those coefficients for the powers $\langle \bar{P}_{\text{QD+NP}}^{(F)} \rangle_{\psi_e, \theta_e, \varphi_e}$ emitted by the system QD + NP and averaged both over the period $T = 2\pi/\omega$ and the Euler angles (over the orientation of the crystal lattice in the QD or, equivalently, over the QD arrangements near the NP) are given in Appendix 2 (for bright exciton states with the quantum number $F = 1$ of the total angular momentum) and in Appendix 3 (for dark exciton states with $F = 2$).

642

8. Calculation of the Intensity of EM Field Energy Absorption by a Metal NP

Electrons in the NP absorb the EM field energy. For the EM field emitted by a QD exciton state with the quantum number F of the total angular momentum, the intensity $\bar{Q}_{\text{NP}}^{(F)}$ of its absorption by the metal NP (the energy absorbed by the NP per unit time), which is averaged over the period $T = 2\pi/\omega$, can be calculated using the formula

$$\begin{aligned} \bar{Q}_{\text{NP}}^{(F)} &= \int_{\text{NP}} \overline{[\mathbf{j}(\mathbf{r}, t; F)]_{\text{Re}} \cdot [\mathbf{E}_1^{\text{NP}}(\mathbf{r}, t; F)]_{\text{Re}}} d^3r = \\ &= \frac{\omega}{8\pi} \int_{\text{NP}} \left\{ \text{Im}(\varepsilon_1^T(\omega, 0)) |\mathbf{E}_{1,T}^{\text{NP}}(\mathbf{r}; F)|^2 + \text{Re}(\varepsilon_1^T(\omega, 0)) \times \right. \\ &\times \text{Im} \left[\mathbf{E}_{1,T}^{\text{NP}}(\mathbf{r}; F) \cdot (\mathbf{E}_{1,L}^{\text{NP}}(\mathbf{r}; F))^* \right] + \text{Im}(\varepsilon_1^T(\omega, 0)) \times \\ &\times \text{Re} \left[\mathbf{E}_{1,T}^{\text{NP}}(\mathbf{r}; F) \cdot (\mathbf{E}_{1,L}^{\text{NP}}(\mathbf{r}; F))^* \right] \left. \right\} d^3r, \quad (45) \end{aligned}$$

where

$$[\mathbf{A}(\mathbf{r}, t)]_{\text{Re}} = [\mathbf{A}(\mathbf{r}) \exp(-i\omega t) + \mathbf{A}^*(\mathbf{r}) \exp(i\omega t)]/2,$$

$\mathbf{j}(\mathbf{r}, t; F)$ is the current density of electrons, $\mathbf{E}_{1,T}^{\text{NP}}(\mathbf{r}, t; F)$ and $\mathbf{E}_{1,L}^{\text{NP}}(\mathbf{r}, t; F)$ are the transverse and longitudinal, respectively, electric fields in the NP (the corresponding expressions for these fields in the form of their multipole expansions can be found in work [3]), the wave number $k_L(\omega)$ of longitudinal oscillations is determined from the condition $\varepsilon_1^L(\omega, k_L) = 0$, and the wave number $k_T(\omega)$ of transverse oscillations is defined by the dispersion equation $k_T^2 = \varepsilon_1^T(\omega, 0) \omega^2/c^2$. For the record of the further formulas to be compact, the following notation will be useful:

$$\begin{aligned} t_l^E &= |V_{E,31}^{\text{NP}}(l)|^2 \frac{\text{Im}[\varepsilon_{pl}^T(\omega, 0)]}{|\varepsilon_1^T(\omega, 0)|^2 (k_0 R_1)^2} \times \\ &\times \int_0^1 \left\{ l(l+1) |j_l(k_T R_1 x)|^2 + \left| [y j_l(y)]'_{y=k_T R_1 x} \right|^2 \right\} dx, \quad (46) \end{aligned}$$

$$\begin{aligned} \alpha_l &= \int_0^1 \left\{ j_l(k_T R_1 x) [y j_l'(y)]'_{y=k_L R_1 x} + \right. \\ &+ \left. [y j_l(y)]'_{y=k_T R_1 x} j_l^*(k_L R_1 x) \right\} dx, \quad (47) \end{aligned}$$

$$\beta_l = \frac{V_{E,31}^{\text{NP}}(l) (V_{L,31}^{\text{NP}}(l))^*}{\varepsilon_1^T(\omega, 0) k_L^* R_1}, \quad (48)$$

$$t_l^{E,L} = t_l^E - \frac{\sqrt{l(l+1)}}{k_0 R_1} \left\{ \text{Re}[\varepsilon_1^T(\omega, 0)] [\beta_l' \alpha_l'' + \beta_l'' \alpha_l'] + \right.$$

$$+ \text{Im}[\varepsilon_{pl}^T(\omega, 0) + \varepsilon_{pl}^L(\omega, k_L)] [\beta_l' \alpha_l' - \beta_l'' \alpha_l''] \}, \quad (49)$$

$$t_l^M = |V_{M,31}^{\text{NP}}(l)|^2 \text{Im}[\varepsilon_{pl}^T(\omega, 0)] \int_0^1 |j_l(k_T R_1 x)|^2 x^2 dx. \quad (50)$$

In expressions (46)–(47), the primed quantities mean the derivative with respect to the argument, the single- and double-primed α_l , and β_l in expression (49) mean the real and imaginary, respectively, parts of those quantities, and $V_{E,31}^{\text{NP}}(l)$, $V_{M,31}^{\text{NP}}(l)$, and $V_{L,31}^{\text{NP}}(l)$ are the coupling amplitudes between the coefficients in the multipole expansions of the EM field outside and inside the NP [3]. Introducing the quantities

$$X_{l,n}^{(m)} = t_l^{E,L} |M_{k+l,n}^{(m)}|^2 + t_l^M |M_{l,n}^{(m)}|^2, \quad (51)$$

$$W_{l,n,j}^{(m)} = t_l^{E,L} M_{k+l,n}^{(m)} (M_{k+l,j}^{(m)})^* + t_l^M M_{l,n}^{(m)} (M_{l,j}^{(m)})^*, \quad (52)$$

the intensities $\langle \overline{Q}_{\text{NP}}^{(F)} \rangle_{\psi_e, \theta_e, \varphi_e}$ of the absorption of the EM field energy by the metal NP averaged over the period $T = 2\pi/\omega$ and the Euler angles can be written in the form

$$\langle \overline{Q}_{\text{NP}}^{(1)} \rangle_{\psi_e, \theta_e, \varphi_e} = \frac{\omega |p|^2 k_0^3}{108} \varepsilon_2^{3/2} (k_0 R_1)^3 S_{Q,1}, \quad (53)$$

$$\langle \overline{Q}_{\text{NP}}^{(2)} \rangle_{\psi_e, \theta_e, \varphi_e} = \frac{\omega |p|^2 k_0^3}{450} I_2^2 \varepsilon_2^{3/2} (k_0 R_1)^3 S_{Q,2}, \quad (54)$$

where $S_{Q,1}$ and $S_{Q,2}$ are the sums in formulas (A2.1) and (A3.1), respectively, but with the coefficients $X_{l,n}^{(m)}$ instead of $B_{l,n}^{(m)}$, and $W_{l,n,j}^{(m)}$ instead of $C_{l,n}^{(m)}$.

9. Calculation of Excitonic Emission Rates, Non-radiative Losses, and Emission Quantum Yield in the Nanosystem QD + NP

While calculating the emission characteristics of the hybrid nanosystems QD + NP, the quasiequilibrium character of the dark and bright exciton level populations at finite temperatures has to be taken into account. The total averaged emission power $\langle P_{\text{QD}} \rangle$ of a single semiconductor QD can be written as

$$\langle P_{\text{QD}} \rangle = \frac{\overline{P}_{\text{QD}}^{(2)} + \overline{P}_{\text{QD}}^{(1)} \exp(-\Delta/k_B T)}{1 + \exp(-\Delta/k_B T)}, \quad (55)$$

where $\Delta(R_2)$ is the splitting of dark and bright exciton levels (see Section 5). The total averaged emission power $\langle P_{\text{QD+NP}} \rangle$ of the nanosystems QD + NP is expressed analogously to formula (55), but with $\overline{P}_{\text{QD}}^{(1)}$

substituted by $\langle \overline{P}_{\text{QD+NP}}^{(1)} \rangle_{\psi_e, \theta_e, \varphi_e}$ (Eq. (A2.1)), and $\overline{P}_{\text{QD}}^{(2)}$ by $\langle \overline{P}_{\text{QD+NP}}^{(2)} \rangle_{\psi_e, \theta_e, \varphi_e}$ (Eq. (A3.1)). Performing the substitutions $\langle P_{\text{QD}} \rangle$ by $\langle Q_{\text{NP}} \rangle$, $\overline{P}_{\text{QD}}^{(2)}$ by $\langle \overline{Q}_{\text{NP}}^{(2)} \rangle_{\psi_e, \theta_e, \varphi_e}$, and $\overline{P}_{\text{QD}}^{(1)}$ by $\langle \overline{Q}_{\text{NP}}^{(1)} \rangle_{\psi_e, \theta_e, \varphi_e}$ in formula (55), an analogous expression can also be obtained for the total intensity of absorption of the QD-emitted EM field energy by the metal NP.

Let the calculation parameters be the rate of non-radiative losses $\gamma_{\text{nr}}^{\text{QD}}$ (the rate of non-radiative recombination) and the quantum yield of excitonic emission by a single QD, $\eta_{\text{QD}} = \gamma_r^{\text{QD}} / (\gamma_r^{\text{QD}} + \gamma_{\text{nr}}^{\text{QD}})$. Typical values of the former in the case of a CdTe QD are $\gamma_{\text{nr}}^{\text{QD}} \sim (2 \div 7) \times 10^7 \text{ s}^{-1}$ [27, 28]. Thereby, we also selected the rate of radiative exciton recombination in the isolated QD, $\gamma_r^{\text{QD}} = \gamma_{\text{nr}}^{\text{QD}} \eta_{\text{QD}} / (1 - \eta_{\text{QD}})$. It is clear that the power $\langle P_{\text{QD}} \rangle$ emitted by an isolated semiconductor QD has to be proportional to the rate of radiative recombination γ_r^{QD} : $\langle P_{\text{QD}} \rangle / \hbar \omega = A_r \gamma_r^{\text{QD}}$. Having determined the coefficient A_r from this equality, we can determine the rate of excitonic emission by the nanosystem QD + NP in whole, $\gamma_r^{\text{QD+NP}} = \langle P_{\text{QD+NP}} \rangle / (A_r \hbar \omega)$, and the rate of non-radiative losses in this system, $\gamma_{\text{nr}}^{\text{QD+NP}} = \gamma_{\text{nr}}^{\text{QD+NP}} + \gamma_{\text{nr, FRET}}^{\text{QD+NP}}$, where $\gamma_{\text{nr}}^{\text{QD+NP}} = \gamma_{\text{nr}}^{\text{QD}} + \langle Q_{\text{NP}} \rangle / (A_r \hbar \omega)$, and $\gamma_{\text{nr, FRET}}^{\text{QD+NP}}$ is a contribution from the direct resonance transmission of the exciton energy to a plasmon excitation in the NP without the participation of photons. This contribution, which decreases, as the distance D between the QD and the NP increases, as D^{-6} in the dipole approximation, is calculated in the framework of the model [29].

In Fig. 6, the calculated dependences of the radiative recombination rate $\gamma_r^{\text{QD+NP}}$ and the rates of non-radiative losses $\gamma_{\text{nr}}^{\text{QD+NP}}$ and $\gamma_{\text{nr, FRET}}^{\text{QD+NP}}$ on the distance $h = D - R_1 - R_2$ between the surface of a CdTe QD and the surface of a silver or gold NP (D is the distance between the NP and QD centers) are depicted for QD diameters of 2.5 and 3.5 nm, an NP diameter of 70 nm, the quantum yield of isolated QD $\eta_{\text{QD}} = 10\%$, and $T = 300 \text{ K}$. The relevant dependence for the rate of non-radiative losses $\gamma_{\text{nr, FRET}}^{\text{QD+NP}}$ in the case of a silver NP is not shown because of its small values $\gamma_{\text{nr, FRET}}^{\text{QD+NP}} < 3 \times 10^6 \text{ s}^{-1}$.

In Figs. 7 to 10, the dependences of the relative emission quantum yield $\eta_{\text{rel}} = \eta_{\text{QD+NP}} / \eta_{\text{QD}}$ on the distance between the QD and NP surfaces are shown for the cases of silver and gold NPs at temperatures of

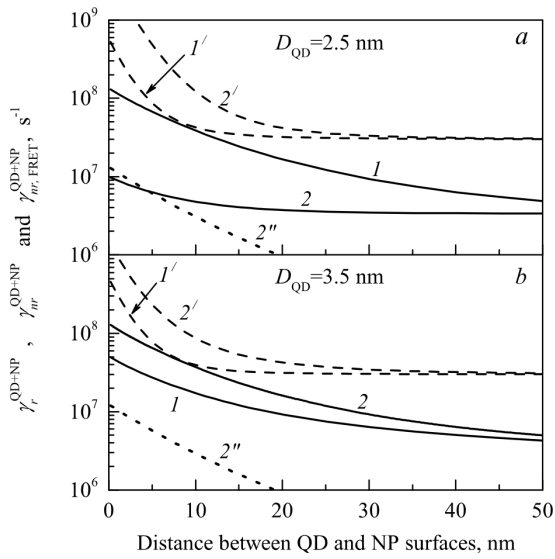


Fig. 6. Dependences of the radiative recombination rate $\gamma_{r, \text{QD+NP}}^{\text{QD+NP}}$ (curves 1 and 2) and the rates of non-radiative losses $\gamma_{\text{nr, FRET}}^{\text{QD+NP}}$ (curves 1' and 2') and $\gamma_{\text{nr}}^{\text{QD+NP}}$ (curve 2'') on the distance between the surface of CdTe QD 3 (panel a) and 3.5 nm (panel b) in diameter and the surface of a silver (curves 1 and 1') or gold (curves 2, 2', and 2'') NP 70 nm in diameter. Calculation parameters: $\gamma_{\text{nr}}^{\text{QD}} = 3 \times 10^7 \text{ s}^{-1}$, $\eta_{\text{QD}} = 10\%$, and $T = 300 \text{ K}$

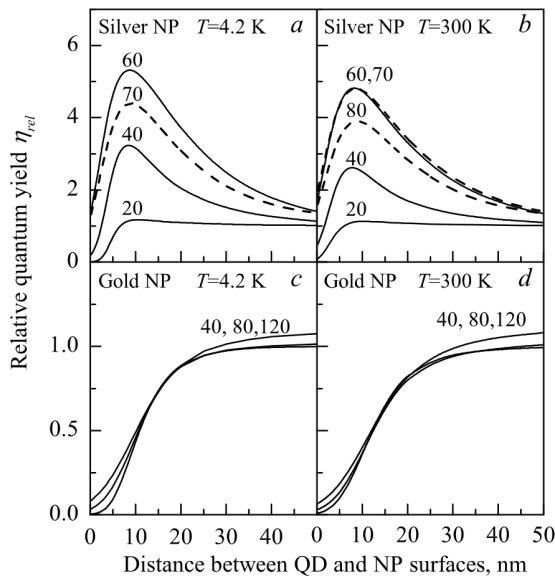


Fig. 7. Dependences of the relative emission quantum yield of the nanosystem “semiconductor QD + metal NP” on the distance between the QD and NP surfaces for QD 2 nm in diameter: silver NP and $T = 4.2$ (a) and 300 K (b); gold NP and $T = 4.2$ (c) and 300 K (d). The NP diameter (in nanometers) is indicated near the corresponding curve

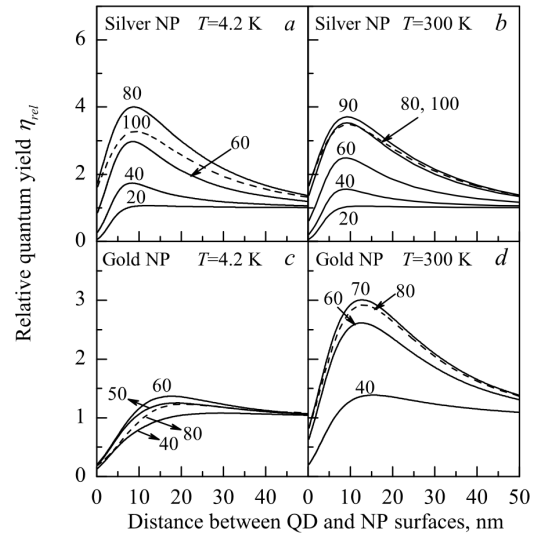


Fig. 8. The same as in Fig. 7, but for QD 3 nm in diameter

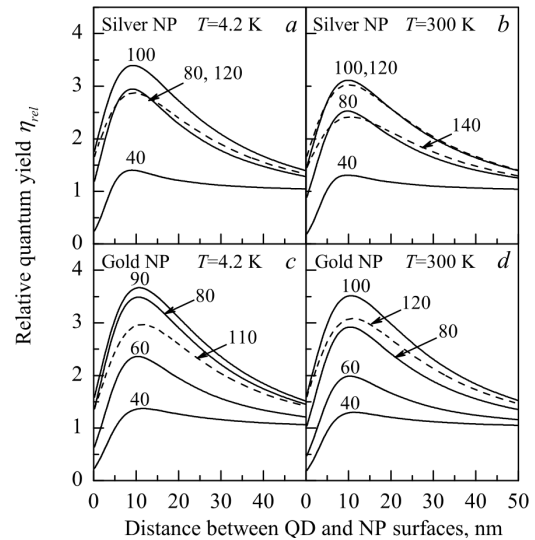


Fig. 9. The same as in Fig. 7, but for QD 3.5 nm in diameter

4.2 and 300 K for various QD and NP sizes, provided the emission quantum yield for the isolated QD equal $\eta_{\text{QD}} = 10\%$. A substantial increase of the emission quantum yield in the case of a gold NP and the QD sizes $D_{\text{QD}} = 2R_2 \gtrsim 3.5 \text{ nm}$ is related to the fact that, at such QD dimensions, the energies of exciton transitions (see Fig. 2) fall within the energy interval of interface plasmons in the gold NP (see Fig. 4), which gives rise to the emergence of a resonance in the exciton-plasmon interaction.

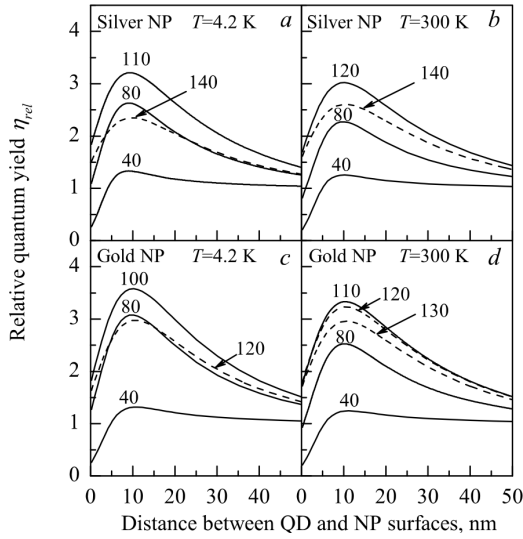


Fig. 10. The same as in Fig. 7, but for QD 5 nm in diameter

Similar dependences of the relative emission quantum yield on the distance between the NP and QD surfaces in the case where the quantum yield for a single QD is $\eta_{\text{QD}} = 50\%$ demonstrate maximal values $\eta_{\text{rel}}^{\text{max}}$ in the range 1.3–1.5 at larger separation distances (~ 16 nm in the case of silver NP and 20–25 nm in the case of gold NP).

10. Conclusions

A model of excitonic emission by a non-spherical nanosystem “emitting spherical semiconductor QD + spherical metal NP” has been developed in the case of a semiconductor with cubic modification and a fourfold degenerate valence band Γ_8 . The multiple scattering of the electromagnetic field, which is emitted by dark and bright excitons in the QD, between the QD and the NP is taken into account. The emitted power and the rate of radiative recombination, as well as the absorption intensity and the rate of non-radiative energy losses in the system are calculated. This made it possible to determine the emission quantum yield and its dependence on the distance between the NP and the QD, the NP and QD sizes, the temperature, and other parameters. It is shown that, unlike the electromagnetic field emitted by a point dipole in a vicinity of the metal NP, which contains the infinite number of multipole components, the electromagnetic field emitted by the QD contains only the dipole and octupole components of the elec-

tric type and the quadrupole components of the magnetic type. As a result, the absorption of the EM field energy by interface plasmons in the metal NP in the QD + NP nanosystem is considerably lower than in the case of a point dipole in a vicinity of the NP, when the multipole components of higher orders give the main contribution to the absorption at small distances between the point dipole and the metal NP [30–32]. As a consequence, the emission quantum yield of a QD in a vicinity of the metallic NP is higher than that of an imaginary point dipole located at the same distance from the metallic NP surface as that to the QD center, the emission parameters (including the frequency) of the dipole being the same as those of the appropriate QD.

The authors express their sincere gratitude to the Acting Director of the V.E. Lashkaryov Institute of Semiconductor Physics of the National Academy of Sciences of Ukraine Corresponding Member of the NANU O.E. Belyaev for his support and discussion of the results of this work. The work was carried out in the framework of the complex goal-oriented program for fundamental researches at the NAS of Ukraine “Fundamental problems of nanostructural systems, nanomaterials, nanotechnologies” 2010–2014 (theme No. 52/7/47).

APPENDIX 1

$$C_{2,0} = -\sqrt{3/8} \exp(-2i\varphi_e) \sin^2 \theta_e, \quad C_{-2,0} = C_{2,0}^*, \quad (\text{A1.1})$$

$$C_{2,\pm 1} = \mp i \exp(-2i\varphi_e \mp i\Psi_e) \sin \theta_e \frac{1 \pm \cos \theta_e}{2}, \quad (\text{A1.2})$$

$$C_{-2,\pm 1} = -C_{2,\mp 1}^*, \quad (\text{A1.3})$$

$$C_{2,\pm 2} = \exp(-2i\varphi_e \mp 2i\Psi_e) (1 \pm \cos \theta_e)^2 / 4, \quad (\text{A1.4})$$

$$C_{-2,\pm 2} = C_{2,\mp 2}^*, \quad (\text{A1.5})$$

$$C_{1,0} = -i\sqrt{3/2} \exp(-i\varphi_e) \sin \theta_e \cos \theta_e, \quad (\text{A1.6})$$

$$C_{-1,0} = -C_{1,0}^*, \quad (\text{A1.7})$$

$$C_{1,\pm 1} = \exp(-i\varphi_e \mp i\Psi_e) (1 \pm \cos \theta_e) \times \quad (\text{A1.8})$$

$$\times (\pm \cos \theta_e - 1/2), \quad C_{-1,\pm 1} = C_{1,\mp 1}^*, \quad (\text{A1.9})$$

$$C_{1,\pm 2} = \mp i \exp(-i\varphi_e \mp 2i\Psi_e) \sin \theta_e \times \quad (\text{A1.10})$$

$$\times (1 \pm \cos \theta_e) / 2, \quad C_{-1,\pm 2} = -C_{1,\mp 2}^*, \quad (\text{A1.11})$$

$$C_{0,0} = (3 \cos^2 \theta_e - 1) / 2, \quad (\text{A1.12})$$

$$C_{0,\pm 1} = -i\sqrt{3/2} \exp(\mp i\Psi_e) \sin \theta_e \cos \theta_e, \quad (\text{A1.13})$$

$$C_{0,\pm 2} = -\sqrt{3/8} \exp(\mp 2i\Psi_e) \sin^2 \theta_e. \quad (\text{A1.14})$$

APPENDIX 2

$$\langle \bar{P}_{\text{QD+NP}}^{(1)} \rangle_{\Psi_e, \theta_e, \varphi_e} = \frac{\omega |p|^2 k_0^3}{108} \left(\frac{\varepsilon_2}{\varepsilon_3} \right)^{3/2} \sum_{l=1}^k \left\{ \sqrt{\varepsilon_2} \times \right.$$

$$\begin{aligned}
 & \times |V_{E,23}^{\text{QD}}(1)|^2 I_0^2 \left[B_{l,k+1}^{(0)} \left(10 - 2 \frac{I_2}{I_0} + \frac{13}{8} \frac{I_2^2}{I_0^2} \right) + \right. \\
 & + B_{l,k+1}^{(1)} \left(14 - 6 \frac{I_2}{I_0} + \frac{39}{8} \frac{I_2^2}{I_0^2} \right) + \\
 & + \sqrt{\varepsilon_2} |V_{E,23}^{\text{QD}}(3)|^2 \frac{I_2^2}{56} \left[234 B_{l,k+3}^{(0)} + 597 B_{l,k+3}^{(1)} + \right. \\
 & + 390 B_{l,k+3}^{(2)} \theta(l-2) + 315 B_{l,k+3}^{(3)} \theta(l-3) \left. \right] + \\
 & + \frac{|V_{M,23}^{\text{QD}}(2)|^2}{\sqrt{\varepsilon_2}} \frac{147}{250} I_2^2 \left[12 B_{l,2}^{(0)} + 19 B_{l,2}^{(1)} + 13 B_{l,2}^{(2)} \theta(l-2) \right] + \\
 & + \sqrt{\varepsilon_2} \sqrt{3/7} I_0 I_2 \text{Re} \left(V_{E,23}^{\text{QD}}(1) \left[V_{E,23}^{\text{QD}}(3) \right]^* (1+i) \tilde{I} \times \right. \\
 & \times \left[\sqrt{\frac{3}{2}} C_{l,k+1,k+3}^{(0)} + \frac{13}{2} C_{l,k+1,k+3}^{(1)} \right] \left. \right) + \\
 & + \frac{42}{5\sqrt{15}} I_0 I_2 \text{Re} \left(V_{E,23}^{\text{QD}}(1) \left[V_{M,23}^{\text{QD}}(2) \right]^* (2-i) \tilde{I} C_{l,k+1,2}^{(1)} \right) + \\
 & + \frac{21}{20\sqrt{14}} I_2^2 \text{Re} \left(V_{E,23}^{\text{QD}}(3) \left[V_{M,23}^{\text{QD}}(2) \right]^* (1-3i) \times \right. \\
 & \times \left. \left[\frac{11}{\sqrt{10}} C_{l,k+3,2}^{(1)} + C_{l,k+3,2}^{(2)} \theta(l-2) \right] \right) \left. \right\}, \quad (\text{A2.1})
 \end{aligned}$$

where

$$\tilde{I} = 1 - \frac{I_2}{I_0} \left(\frac{1}{2} + \frac{3}{4} i \right). \quad (\text{A2.2})$$

APPENDIX 3

$$\begin{aligned}
 \langle \bar{P}_{\text{QD+NP}}^{(2)} \rangle_{\Psi_{e,\theta_e,\varphi_e}} &= \frac{\omega |p|^2 k_0^3}{450} \left(\frac{\varepsilon_2}{\varepsilon_3} \right)^{3/2} I_2^2 \times \\
 & \times \sum_{l=1}^k \left\{ \sqrt{\varepsilon_2} |V_{E,23}^{\text{QD}}(1)|^2 \frac{3}{2} \left[B_{l,k+1}^{(0)} + 3 B_{l,k+1}^{(1)} \right] + \right. \\
 & + \sqrt{\varepsilon_2} \frac{|V_{E,23}^{\text{QD}}(3)|^2}{56} \left[138 B_{l,k+3}^{(0)} + 329 B_{l,k+3}^{(1)} + \right. \\
 & + 326 B_{l,k+3}^{(2)} \theta(l-2) + 231 B_{l,k+3}^{(3)} \theta(l-3) \left. \right] + \\
 & + \frac{|V_{M,23}^{\text{QD}}(2)|^2}{\sqrt{\varepsilon_2}} \frac{49}{200} \left[75 B_{l,2}^{(0)} + 112 B_{l,2}^{(1)} + \right. \\
 & + 133 B_{l,2}^{(2)} \theta(l-2) - \sqrt{\varepsilon_2} \sqrt{\frac{3}{112}} \text{Re} \left(V_{E,23}^{\text{QD}}(1) \times \right. \\
 & \times \left[V_{E,23}^{\text{QD}}(3) \right]^* (1+i) \left[\sqrt{6} C_{l,k+1,k+3}^{(0)} + \right. \\
 & + 13 C_{l,k+1,k+3}^{(1)} \left. \right] - \sqrt{\frac{147}{125}} \text{Re} \left(V_{E,23}^{\text{QD}}(1) \times \right. \\
 & \times \left[V_{M,23}^{\text{QD}}(2) \right]^* (2-i) C_{l,k+1,2}^{(1)} \left. \right) + \frac{1}{20} \sqrt{\frac{7}{5}} \times \\
 & \times \text{Re} \left(V_{E,23}^{\text{QD}}(3) \left[V_{M,23}^{\text{QD}}(2) \right]^* \left[(1-63i) C_{l,k+3,2}^{(1)} + \right. \right. \\
 & \left. \left. + \sqrt{10} (-13-45i) C_{l,k+3,2}^{(2)} \theta(l-2) \right] \right) \left. \right\}. \quad (\text{A3.1})
 \end{aligned}$$

1. N.C. Bigall, W.J. Parak, and D. Dorfs, *Nano Today* **7**, 282 (2012).
2. R. Jiang, B. Li, C. Fang, and J. Wang, *Adv. Mater.* **26**, 5274 (2014).

3. Yu.V. Kryuchenko and D.V. Korbutyak, *Semicond. Phys. Quant. Electr. Optoelectr.* **16**, 227 (2013).
4. Al.L. Efros, M. Rosen, M. Kuno, M. Nirmal, D.J. Norris, and M. Bawendi, *Phys. Rev. B* **54**, 4843 (1996).
5. L.D. Landau and E.M. Lifshitz, *Quantum Mechanics. Non-Relativistic Theory* (Pergamon Press, New York, 1977).
6. R.S. Knox, *Theory of Excitons* (Academic Press, New York, 1964).
7. S. Flügge, *Practical Quantum Mechanics* (Springer, Berlin, 1971), Vol. 1.
8. O. Madelung, *Semiconductors: Data Handbook* (Springer, Berlin, 2004).
9. J.D. Jackson, *Classical Electrodynamics* (Wiley, New York, 1962).
10. H. Bateman and A. Erdelyi, *Tables of Integral Transforms* (McGraw-Hill, New York, 1954), Vol. 2.
11. J.H. Blokland, V.I. Claesse, F.J.P. Wijnen *et al.*, *Phys. Rev. B* **83**, 035304 (2011).
12. P. Yang and N. Murase, *J. Phys.: Conf. Ser.* **152**, 012009 (2009).
13. L. Jing, L. Yang, R. Qiao, M. Niu, M. Du, D. Wang, and M. Gao, *Chem. Mater.* **22**, 420 (2010).
14. P. Reineck, D. Gomez, S.H. Ng, M. Karg, T. Bell, P. Mulvaney, and U. Bach, *ACS Nano* **7**, 6636 (2013).
15. L. Tang, J. Xu, P. Guo, X. Zhuang, Y. Tian, Y. Wang, H. Duan, and A. Pan, *Opt. Express* **21**, 11095 (2013).
16. D. Ban, J. Xue, R. Fang, S. Xu, E. Lu, and P. Xu, *J. Vac. Sci. Technol. B* **16**, 989 (1998).
17. I.M. Kupchak, D.V. Korbutyak, Yu.V. Kryuchenko, A.V. Sachenko, I.O. Sokolovskii, O.M. Sreseli, *Semiconductors* **40**, 94 (2006).
18. Z.A. Weinberg, *J. Appl. Phys.* **53**, 5052 (1982).
19. C. Wood and D. Jena, *Polarization Effects in Semiconductors: From Ab Initio Theory to Device Applications* (Springer, Berlin, 2008).
20. W.W. Yu, L. Qu, W. Guo, and X. Peng, *Chem. Mater.* **15**, 2854 (2003).
21. V.V. Klimov, *Nanoplasmonics* (Nauka, Moscow, 2012) (in Russian).
22. V.V. Datsyuk, *Ukr. J. Phys.* **56**, 122 (2011).
23. P.G. Etchegoin, E.C. Le Ru, and M. Meyer, *J. Chem. Phys.* **125**, 164705 (2006).
24. C. Sönnichsen, *Ph.D. thesis* (Ludwig Maximilian Univ. of Munich, Munich, 2001).
25. P.B. Johnson and R.W. Christy, *Phys. Rev. B* **6**, 4370 (1972).
26. W.J. Tropic, M.E. Thomas, and T.J. Harris, in *Handbook of Optics*, edited by M. Bass (McGraw-Hill, New York, 1995), Ch. 33.
27. S. Emin, A. Loukanov, M. Wakasa, S. Nakabayashi, and Y. Kaneko, *Chem. Lett.* **39**, 654 (2010).
28. S.J. Byrne, S.A. Corr, T.Y. Rakovich *et al.*, *J. Mater. Chem.* **16**, 2896 (2006).
29. A.O. Govorov, G.W. Bryant, W. Zhang, T. Skeini, J. Lee, N.A. Kotov, J.M. Slocik, and R.R. Naik, *Nano Lett.* **6**, 984 (2006).
30. R. Ruppini, *J. Chem. Phys.* **76**, 1681 (1982).

31. H. Mertens, A.F. Koenderink, and A. Polman, Phys. Rev. B **76**, 115123 (2007).
 32. G. Sun and J.B. Khurgin, IEEE J. Select. Topics Quant. Electr. **17**, 110 (2011).

Received 02.12.14.

Translated from Ukrainian by O.I. Voitenko

Ю.В. Крюченко, Д.В. Корбутяк

ЕКСИТОННЕ ВИПРОМІНЮВАННЯ
 ГІБРИДНОЇ НАНОСИСТЕМИ “СФЕРИЧНА
 НАПІВПРОВІДНИКОВА КВАНТОВА
 ТОЧКА + СФЕРИЧНА МЕТАЛЕВА
 НАНОЧАСТИНКА”

Резюме

Досліджено випадок сферичної квантової точки (КТ) прямозонного напівпровідника кубічної модифікації з чотирикратно виродженою валентною зоною Γ_8 в околі сферичної металеві наночастинки (НЧ). Екситонне випромінювання КТ розглянуто як таке, що формується сумою внесків ви-

промінуючих точкових (вузельних) диполів всередині КТ. Опис несферичної в цілому наносистеми базується на використанні трьох сферичних систем координат і встановленні зв'язку між коефіцієнтами мультипольного розкладу електромагнітних (ЕМ) полів у цих системах координат. Полярні осі першої і другої систем з центрами в НЧ і КТ направлені вздовж лінії, що з'єднує ці центри. Орієнтація третьої системи координат з центром в КТ визначається орієнтацією кристалічної ґратки в КТ. Показано, що на відміну від скалярного потенціалу електричного поля, який індукується екситонним станом в КТ і має вигляд потенціалу точкового диполя, ЕМ поле екситонного випромінювання КТ не може бути представлене у вигляді ЕМ поля випромінювання точкового диполя, оскільки містить лише дипольні, квадрупольні і октупольні компоненти. Враховано багаторазове розсіювання між НЧ і КТ електромагнітного поля, що випромінює КТ. Розраховані залежності квантового виходу екситонного випромінювання від відстані між поверхнями КТ і НЧ при різних розмірах КТ і НЧ і температурах 4,2 і 300 К у випадку КТ CdTe і срібних або золотих НЧ.